Materials and Design 31 (2010) 2071–2077

Contents lists available at ScienceDirect

Materials and Design

journal homepage: www.elsevier.com/locate/matdes

# Dissimilar laser brazing of boron nitride and tungsten carbide

Yoshihisa Sechi [a,b,*], Takuya Tsumura [c], Kazuhiro Nakata [c]

[a] Kagoshima Prefectural Institute of Industrial Technology, 1445-1 Oda, Hayato-cho, Kirishima, Kagoshima 899-5105, Japan
[b] Graduate School of Engineering, Osaka University, 2-1 Yamadaoka, Suita, Osaka 565-0871, Japan
[c] Joining and Welding Research Institute, Osaka University, 11-1 Mihogaoka Ibaraki, Osaka 567-0067, Japan

ARTICLE INFO

*Article history:*
Received 26 May 2009
Accepted 4 October 2009
Available online 9 October 2009

*Keywords:*
Laser brazing
Boron nitride
Tungsten carbide

ABSTRACT

Using laser brazing process, we made the dissimilar joint of the boron nitride and tungsten carbide with an excellent functionality. In order to investigate the characteristic of joint, observation and structural analysis of its interface by the electron probe micro-analysis (EPMA) and the scanning acoustic microscopy were performed. The wetting property between h-BN and Ag–Cu–Ti braze was excellent, therefore no gaps were seen between them. Moreover, it was suggested that the Ti element, which is the active ingredient in Ag–Cu–Ti braze, reacted with N in h-BN to generate Ti–N composite phase as an interfacial precipitation and the generation of Ti–N composite phase was affected by the concentration of Ti in Ag–Cu–Ti braze. All fracture was formed in h-BN body near the interface and it seemed that the distribution of shear strength of 1.25%Ti to 1.68%Ti was within the margin of variation of bulk strength of h-BN.


## 1. Introduction

Boron nitride has a various functional characteristics. Especially h-BN has a good thermal resistibility and solid-lubrication [1]. Besides, tungsten carbide/cobalt alloy made by powder metallurgy has low thermal expansion coefficient and high rigidity good for a counter structural material to ceramic. However, only a few researches have done focusing on the joining of boron nitride and tungsten carbide alloy or other metals [2,3] by brazing in a furnace that needs long heating time.

The brazing technology is commonly used for the bonding of ceramic to metals [4–12]. Although, there are some problems such as causing the joint defect that due to thermal stress in the joint field and material deterioration by heating in these dissimilar joining [13].

Among brazing processes [14], laser brazing [4,12,15–28] has good characteristics for dissimilar joining process because of possibility of short heating time and small heating area, and suppression of damage to the base materials without furnace in comparison with conventional furnace brazing. So, this study described dissimilar laser brazing of boron nitride (h-BN) and tungsten carbide, and in order to investigate the characteristic of dissimilar joint, cross-section observation, elemental and structural analyses of joint interface and adhesion evaluation, and shear strength measurement were performed.

## 2. Experimental method

Commercially available tungsten carbide equivalent material classified with ISO K10 grade and high purity h-BN made by hot pressing method without using sintering additives were used in this work. Two types of Silver–Copper–Titanium alloy braze sheet included Ti as major active ingredient for direct ceramic brazing with its thickness were 0.1 mm. Nominal compositions and properties were summarized in Tables 1 and 2. In this report, notations of 1.68%Ti braze and 1.25%Ti braze are used to describe 70.26 mass% Ag–28.06 mass% Cu–1.68 mass% Ti, and 71.07 mass% Ag–27.68 mass% Cu–1.25 mass% Ti, respectively. The size of braze sheet was determined to cover 80% for the joint area of h-BN so that the melted braze not to flow out of the joint.

Before brazing, h-BN block, braze and tungsten carbide plate were degreased by ultrasonic agitation for 10 min in acetone and dried in air.

Sample configuration was a top hat shape. A braze sheet was sandwiched with a h-BN block from top side and a tungsten carbide plate from bottom side in a vacuum chamber. Small pressure of 1.2 MPa was applied to prevent the workpiece from moving when braze sheet was melted, and no gap adjustments for the joint were done. A vacuum chamber with a 100 mm diameter was used in the brazing experiments. This Chamber was evacuated to less than $10^{-1}$ Pa after samples had been loaded, and substitution to the atmospheric pressure with Ar gas was done after the evacuation. The purity of Ar gas was 99.999%. This evacuation and substitution cycles were done at least three times before brazing. During brazing, Ar gas continued to flow, which flow rate was about 5 L/min.

* Corresponding author. Address: Materials Division, Kagoshima Prefectural Institute of Industrial Technology, 1445-1 Oda, Hayato-cho, Kirishima, Kagoshima 899-5105, Japan. Tel.: +81 995 43 5111; fax: +81 995 64 2111.
*E-mail address:* sechi@kagoshima-it.go.jp (Y. Sechi).

0261-3069/$ - see front matter © 2009 Elsevier Ltd. All rights reserved.
doi:10.1016/j.matdes.2009.10.009

**Table 1**
Materials used in this work.

| Material | Grade | Nominal composition (mass%) | Bend strength at room temperature (MPa) | Density ($\times 10^{-3}$ kg/m$^3$) | Relative density (%) | Size (mm) |
|---|---|---|---|---|---|---|
| Tungsten Carbide | HTi 10 | WC: 94, Co: 6 | 32,000 | 14.9 | – | 20 * 20 * 2 |
| h-BN | 99% up | h-BN > 99.993 | 32.5 | 1.93 | 82.5 | 5 * 5 * 3.5 |

**Table 2**
Brazes used in this work.

| Braze | Grade | Nominal composition (mass%) | | | Thickness (mm) |
|---|---|---|---|---|---|
| | | Ag | Cu | Ti | |
| 1.68%Ti | TKC-710 | 70.26 | 28.06 | 1.68 | 0.1 |
| 1.25%Ti | TKC-711 | 71.07 | 27.68 | 1.25 | 0.1 |

Setup of laser brazing was as shown in Fig. 1. The sample was located in a small vacuum chamber. The topside of specimen was covered with a transparent quartz glass plate, which also worked to fix the specimen. The generated YAG and LD lasers were coaxially transferred with an optical fiber to the laser head unit and radiated through the transparent quarts glass plate to the topside of the tungsten carbide plate which radiation angle was 85°. Laser brazing condition was summarized in Table 3. Scanning speed of laser was 0.6 mm/s on the first run and 1.0 mm/s on the second run to the forth run in order to heat the specimen efficiently in a circle around it. In this study, the scanning of laser was done on the tungsten carbide substrate around the h-BN block.

Temperature during laser blazing was monitored at the bottom of tungsten carbide plate using R type thermo couple.

Some of the samples were subsequently cross-sectioned by the low-speed diamond saw with water cooling, and mounted by epoxy resin, curing at room temperature about 8–10 h, and grinded by SiC paper #120–#1200, polished by 3–1 μm polycrystalline diamond to provide microstructural information.

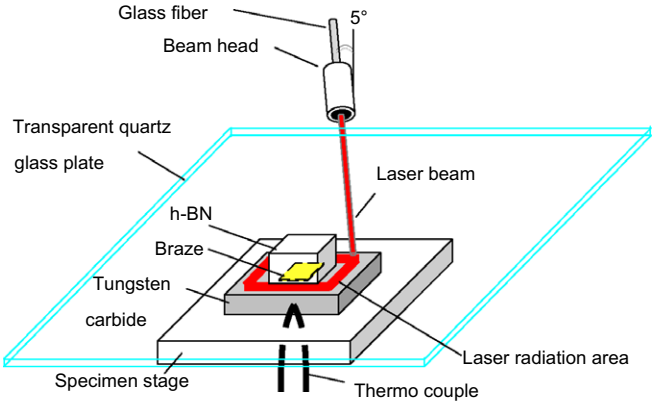


**Fig. 1.** Schematic diagram of laser brazing.

**Table 3**
Laser brazing condition.

| | | |
|---|---|---|
| Pulsed YAG Average Output (kW) | 0.134 | |
| Pulsed YAG wave length (nm) | 1064 | |
| CW LD Output (kW) | 0.02 | |
| CW LD wave length (nm) | 808 | |
| Pulse frequency (Hz) | 100 | |
| Scanning speed (mm/s) | (1st run) | 0.6 |
| | (2nd run) | 1.0 |
| | (3rd run) | 1.0 |
| | (4th run) | 1.0 |
| Laser beam diameter (mm) | 0.5 | |

Cross-sectional observation and elemental analysis of the interface were performed using electron probe micro-analyzer (JEOL Co. Ltd. JXA-8621MX) and X-ray diffractometer (Bruker AXS Co. Ltd. D8: Co Kα). The diameter of collimator was 50 μm to determine crystallographic phase of micro region. Interfacial observation and estimation of interface area were performed using scanning acoustic microscope (Hitachi Kenki FineTech Co., Ltd. HSAM220), which can observe interfacial structure using ultrasonic echo radiated from the prove in a water tank.

Some of the samples were placed in a shearing jig as shown in Fig. 2 and stressed to destruction in precision universal tester (Shimadzu Cooperation Autograph AGS-5kNB) operating at a crosshead speed of 0.5 mm/min.

In order to compensate the effect of interfacial area on the shear strength test, shear strength was calculated from maximum load divided by interface area estimated from scanning acoustic microscopy and its average shear strength was calculated using the Weibull distribution function [29,30]:

$$\ln\ln(1-F)^{-1} = m\ln\sigma - m\ln\sigma_0 \tag{1}$$

where $F$ is the cumulative failure probability, $m$ is the Weibull modulus, $\sigma_0$ is the characteristic strength. In this paper, the median rank method was used for computing cumulative failure probability $F$ in Eq. (1) because of its good reliability despite the small number of samples:

$$F = (i-0.3)/(n+0.4) \tag{2}$$

where $i$ is the rank of the observation and $n$ is the number of samples. Average shear strength $\mu$ is as follows:

$$\mu = \sigma_0\Gamma(1+1/m) \tag{3}$$

where the $\Gamma$ function is expressed as follows:

$$\Gamma(x) = \int_0^\infty e^{-t}t^{x-1}dt \quad (x>0) \tag{4}$$

## 3. Results

### 3.1. h-BN/WC–Co brazed interface structure

Fig. 3 shows the typical profile of the bottom temperature of the WC–Co plate while laser brazing joining. The increase of temperature continued in the approximate proportion of gradient until

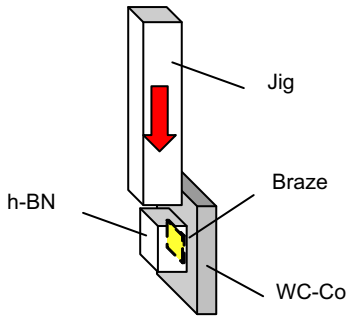


**Fig. 2.** Schematic diagram of shear strength test.

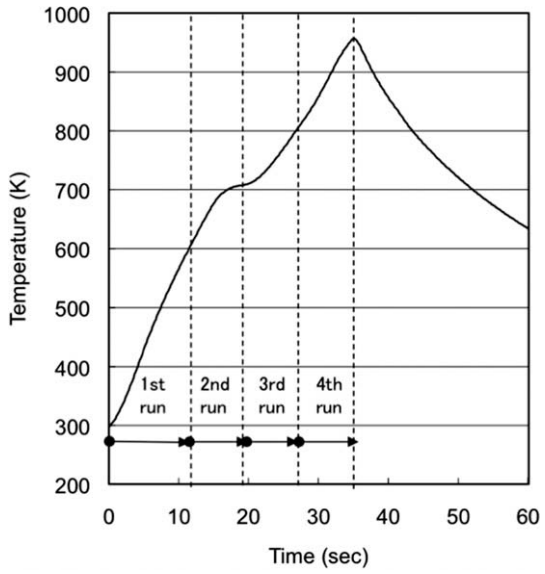


**Fig. 3.** The bottom temperature profile of the WC–Co plate while laser brazing joining.

irradiation of the laser on the forth side. The maximum bottom temperature was around 973 K. After the heating, the bottom temperature decreased quickly to 673 K within 25 s from the end of the forth run of heating. After 100 s from the end of heating, the bottom temperature decreased lower than 400 K.

Fig. 4 shows cross-sectional SEM observation of an h-BN/1.68%Ti braze/WC–Co interface with low magnification. The top and bottom sides of the picture are h-BN and WC–Co, respectively. The intermediate layer is 1.68%Ti braze. Though the contact angle between WC–Co and braze is not measured yet by sessile drop method, it is suggested to be an acute angle from Fig. 3, and the contact angle between h-BN and 1.68%Ti braze is also an acute angle.

Fig. 5 shows cross-sectional SEM observation of an h-BN/1.68%Ti braze/WC–Co interface with high magnification. WC–Co/braze interface is smooth and no voids were observed.

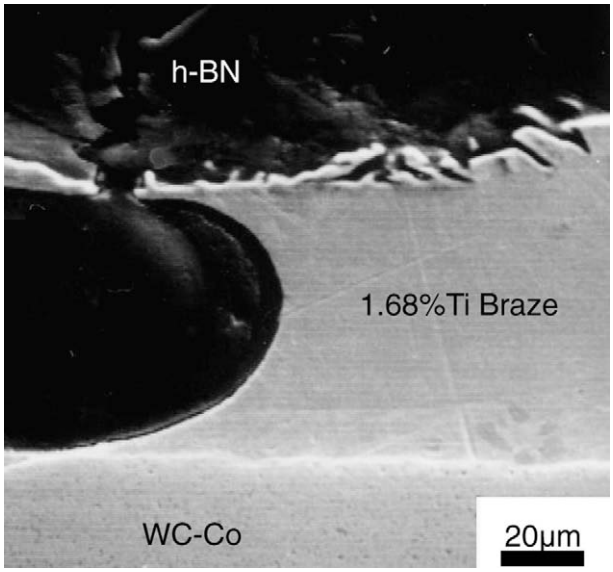


**Fig. 4.** Cross-section of a h-BN/1.68%Ti braze/WC–Co interface.

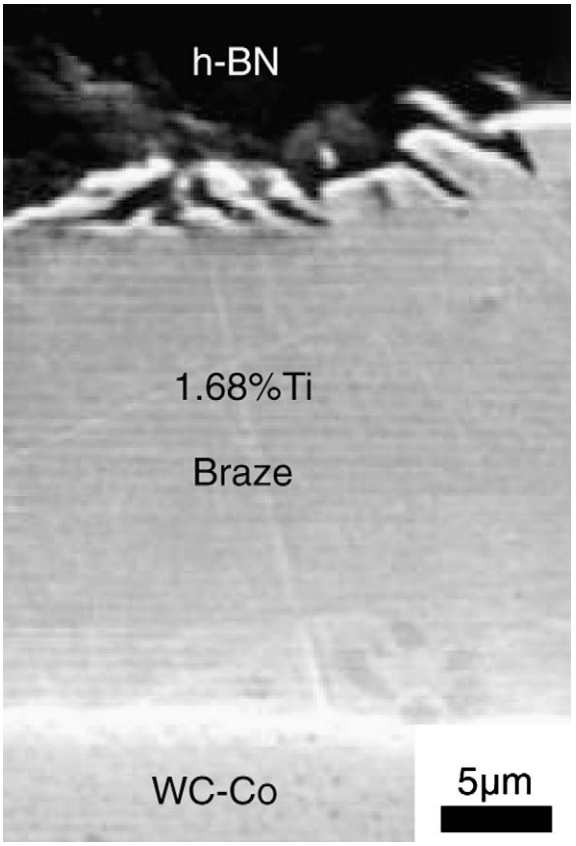


**Fig. 5.** Cross-section of a h-BN/1.68%Ti braze/WC–Co interface (enlargement).

Fig. 6 shows the result of map analysis of an h-BN/1.68%Ti braze interface. Fig. 6a shows enlargement of left and top side of h-BN/Ag–Cu–Ti braze interface in Fig. 5. Fig. 6b shows the distribution of Ag near the interface in the same area of Fig. 6a. Fig. 6c and d shows the distributions of N and Ti, respectively. From these distributions of elements, concentration of Ti near the interface was apparently observed as colored to white in the interface layer of which thickness was about 2 μm.

Fig. 7 shows cross-sectional SEM observation of an h-BN/1.25%Ti braze/WC–Co interface with low magnification. The top and the bottom sides of the picture are h-BN and WC–Co. An intermediate layer is 1.25%Ti braze. The contact angle between WC–Co and 1.25%Ti braze is suggested to be an acute angle from Fig. 7, and the contact angle between h-BN and 1.25%Ti braze is also an acute angle although h-BN surface is not flat with rough surface morphology in comparison with smooth WC–Co/braze interface, which suggests good wettability between them as shown in Fig. 8 with high magnification SEM photo of an h-BN/1.25%Ti braze/WC–Co interface. In Fig. 7, each interface spreads from the right to the left sides.

Fig. 9 shows the results of map analysis of an h-BN/1.25%Ti braze interface, (a) in Fig. 9 shows enlargement of h-BN/1.25%Ti braze interface in Fig. 8. Fig. 9(b–d) shows the distribution of Ag, N and Ti near the interface in the same area of (a), respectively. From these results, the concentration of Ti near the interface was also clearly observed, as the layer of which thickness was about 2 μm.

Fig. 10 shows XRD profiles of the samples at the interface of the h-BN/1.68%Ti braze and h-BN/1.25%Ti braze, respectively. Among strong peaks of h-BN, WC–Co and Ag, which were resulted from bulk ceramics, WC–Co and braze elements, respectively, some peaks from titanium nitrides are found to exist at the interfaces. These weak peaks were indexed as TiN [4,6,9] or $Ti_4N_{3-x}$ [31].

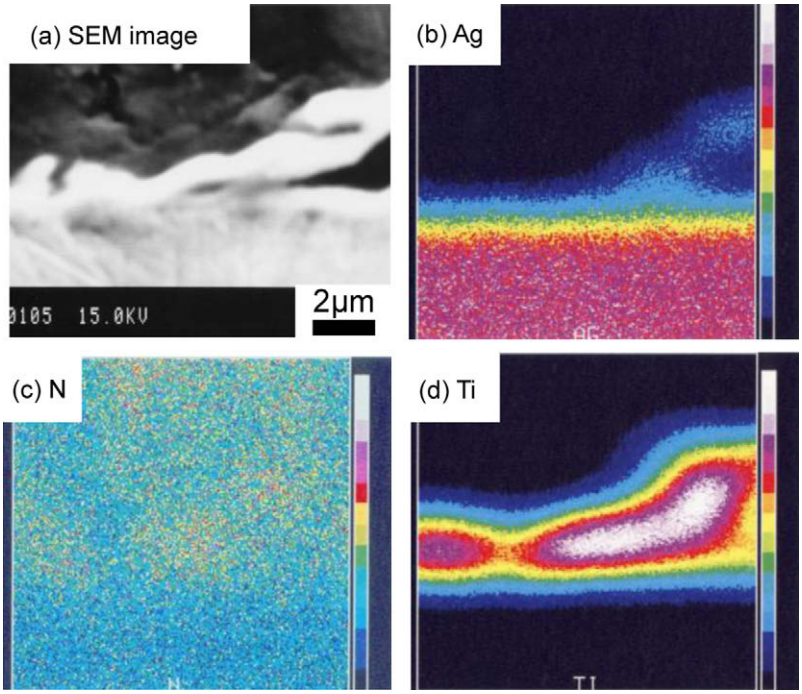


**Fig. 6.** Map analysis of a h-BN/1.68%Ti braze interface.

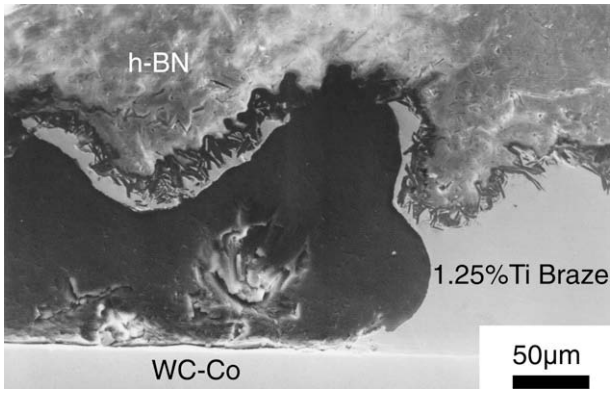


**Fig. 7.** Cross-section of a h-BN/1.25%Ti braze/WC–Co interface.

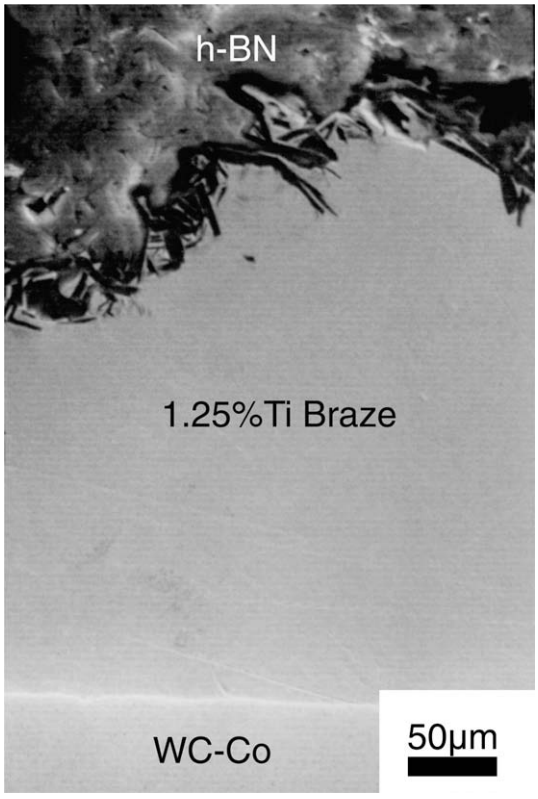


**Fig. 8.** Cross-section of a h-BN/1.25%Ti braze/WC–Co interface(enlargement).

### *3.2. Non-destructive test by scanning acoustic microscopy*

Non-destructive test by scanning acoustic microscopy was done to evaluate how the melted braze filler spread at the interface between h-BN and WC–Co plate. Fig. 11a shows appearance of the specimen and Fig. 11b shows the image of scanning acoustic microscopy at the interface of h-BN/1.68%Ti braze/WC–Co. In Fig. 11a, white part of square in the center is h-BN block, a peripheral metallic luster part is WC–Co. The black area in the center of Fig. 11b is 1.68%Ti braze which was melt at the joint interface and partly spread out of the interface onto WC–Co plate as shown in the upper parts in (a) and (b). However in the white part around the black area, no braze existed. There were no big voids in the black area where melted braze existed at the joint interface.

Fig. 12a shows appearance of the specimen and Fig. 12b shows the image of scanning acoustic microscopy at the interface of h-BN/1.25%Ti braze/WC–Co. In Fig. 12a, white part of square in the center is h-BN block, a peripheral metallic luster part is WC–Co. The black area in the center of Fig. 12b is 1.25%Ti braze which was melt at the joint interface. These characteristics of melted braze using 1.25%Ti were similar to the case using 1.68%Ti braze, while the area of melted braze which spread into the gap between h-BN and WC–Co was smaller than that in case of 1.68%Ti although the volume of braze used had some uneven quantity.

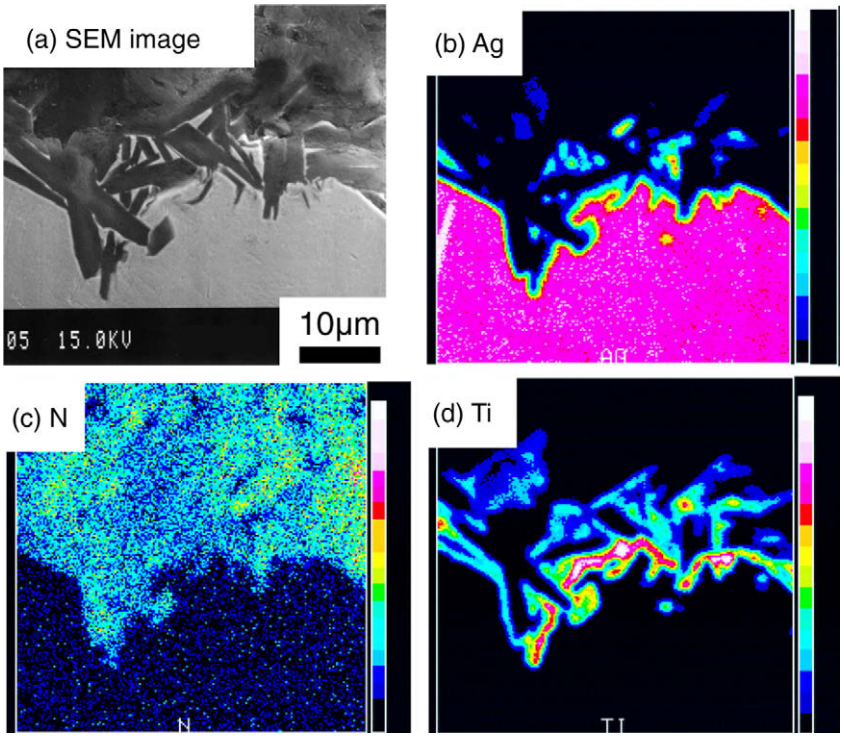


**Fig. 9.** Map analysis of a h-BN/1.25%Ti braze/WC–Co interface.

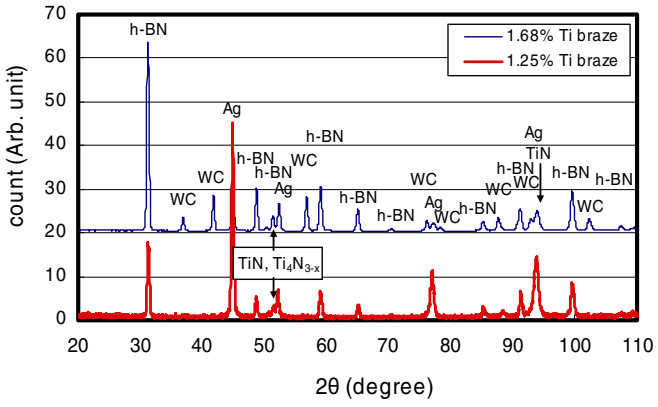


**Fig. 10.** XRD profiles of samples at the interface.

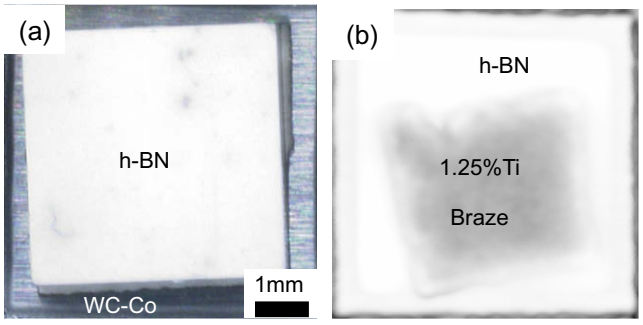


**Fig. 12.** Interface observation of a h-BN/1.25%Ti braze/WC–Co interface using scanning acoustic microscopy.

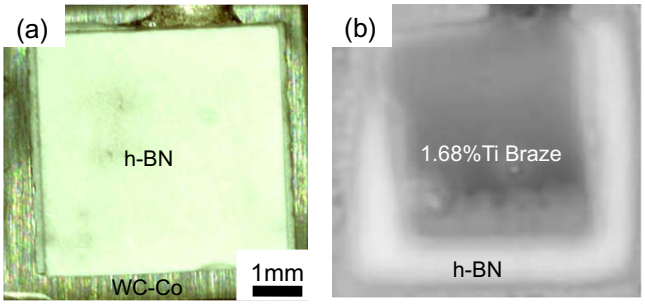


**Fig. 11.** Interface observation of a h-BN/1.68%Ti braze/WC–Co interface using scanning acoustic microscopy.

### 3.3. Shear strength test

After cross-sectional and non-destructive examinations, shear strength test of the dissimilar joint was done. Fig. 13 shows cross-sectional SEM observation of an h-BN/1.68%Ti braze interface after shear strength test has done. The topside is molding epoxy resin. The gray plate-like layer and bottom white colored sides of the picture are h-BN and 1.68%Ti braze, respectively. The upper side of h-BN layer is the fracture surface, while no origins of fracture were observed at the h-BN/1.68%Ti braze interface and braze was melt into the h-BN. In each specimen, fracture occurred at h-BN side of the specimen near the interface. Fig. 14 shows Weibull distributions of shear strength test of h-BN/1.68%Ti braze and h-BN/1.25%Ti braze, respectively, which was plotted using the median rank method. In case of all test, fracture occurred at h-BN side of the specimen near the interface. In both cases, the difference of

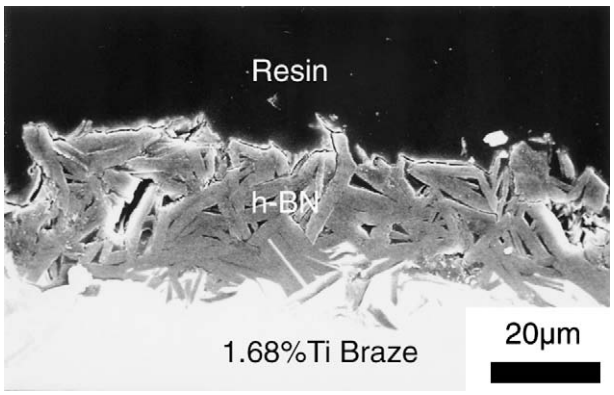


**Fig. 13.** Cross-section of an h-BN/1.68%Ti braze interface after shear strength test.

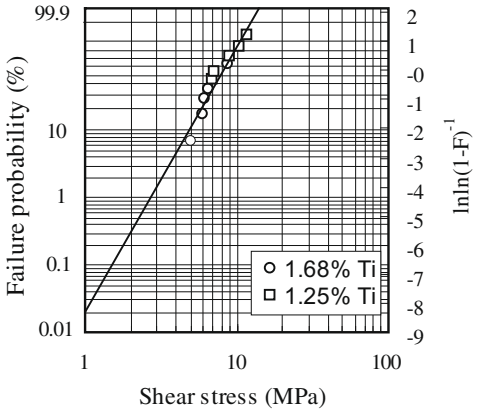


**Fig. 14.** The Weibull distributions of shear strength test.

maximum and minimum shear strength was about 4–5 MPa, respectively. In addition, distributions of shear strength were overlapped each other and spread widely, and can be approximated by line formula as shown.

## 4. Discussions

Fig. 3 shows the maximum bottom temperature during heating was around 973 K. On the other hand, the liquidus temperature of Ag–Cu–Ti braze which was used in this study is 1063 K, and taking the fact that the braze alloy was melt after the heating into consideration, the maximum temperature of topside was thought to be over 1063 K. Thus the difference between the maximum temperature of topside and the maximum bottom temperature seems to arise from thermal decrease in the WC–Co plate due to the distance from the heating area and temperature measuring point.

The contact angle between WC–Co and braze is estimated to be an acute angle from Fig. 4 (using 1.68%Ti braze) and from Fig. 7 (using 1.25%Ti braze). So wettability of Ag–Cu–Ti braze to WC–Co was considered to be good, though accurate measurement with sessile drop method will be needed, and the contact angle between h-BN and Ag–Cu–Ti braze is also estimated to be an acute angle. Wettability of both Ag–Cu–Ti braze to h-BN [6,32,33] was also considered to be good whenever Ti content in braze was even 1.25%. Judging from each interface, WC–Co/Ag–Cu–Ti braze and h-BN/Ag–Cu–Ti braze, spreading to left side, wettability of each interfaces seemed to be good. Nicolas et al. [6] revealed that boron nitride remained unwetted until the temperature was above 1173 K, but wetted at 1223 K by Ag–28%Cu–2%Ti with sessile drop method. So, the result of this study indicates that brazing of h-BN and WC–Co and other metal can be done even using Ag–Cu–Ti alloy in lower than 2%Ti content.

In dissimilar brazing process, vacuum furnace is commonly used to avoid oxidation and its heating rate is relatively slow. But using laser brazing method, good bond strength was achieved because of moving of Ti in Ag–Cu–Ti braze toward the interface and making good reaction of Ti in Ag–Cu–Ti braze and N in h-BN at interface layer in short period within 60 s. Thus, this study shows that braze can be done using rapid heating process.

From Figs. 5 and 8, the interface between WC–Co and Ag–Cu–Ti braze was smooth and no voids were observed [34]. Oppositely, the interface between h-BN and Ag–Cu–Ti braze was very rough in detail. Ag–Cu–Ti braze melted and infiltrated into open pore part of h-BN surface because the wettability between braze and h-BN was excellent. The addition of Ti to braze as an active element seemed to be sufficient to induce wetting of h-BN [6,32,33] even in Ti content of 1.25%.

From Fig. 6a, interface layer existed. In this area, concentrations of Ti and N near the interface were observed from Fig. 6b–d. And Fig. 9 also shows existence of interface layer when using 1.25%Ti braze. The distributions of Ti and N were similar to those of Fig. 6 (using 1.68%Ti braze). These results strongly suggest the formation of reacted layer at the interface of h-BN/Ag–Cu–Ti braze, of which thickness was about 2 μm. From Fig. 10, some small peaks were observed and which were indexed as TiN [4,6,9] or $Ti_4N_{3-x}$ [31] at the interface of the h-BN/1.68%Ti braze and h-BN/1.25%Ti braze, respectively. From Figs. 6 and 9, Ti-rich layers were observed at the interface of h-BN and braze. Thus, these peaks of XRD profile were thought as originated in reacted phase at the interface. Besides, standard free energies of formations of nitrides [35] describes those of TiN and BN at 1173 K are about −220 and −150 (kJ/g mol $N_2$), respectively. Thus judging from standard free energies of formations, TiN is more stable than BN in all temperature ranges. Nicolas et al. [6] reported about the wettability and reactivity of Ti in Ag–28%Cu–2%Ti braze and h-BN. The result of this study agrees with them and in addition, this study shows that the Ti content in Ag–Cu–Ti braze can be reduced to 1.25%. In manufacturing process of Ag–Cu–Ti braze, intermetallic compound phase like $Cu_3Ti$ is produced during melting of raw materials and it increases the hardness of the braze with increasing Ti content. From the point of view about cutting and forming of sheet type braze, it is preferable that the amount of Ti content is small because this intermetallic phase is hard.

As shown in Figs. 11b and 12b, it seemed to be no large voids or cracks in the brazed area. This means that no large defects existed. So the wettability of these braze fillers and h-BN or WC–Co seemed to be good.

In all shear strength tests, every crack was made at h-BN side of the interface of brazing joint as shown in Fig. 13. It suggests that the fracture occurred at base material of h-BN and that the interface of brazing joint has the strength enough to connect h-BN and WC–Co. By using aluminum braze, h-BN failed at its metal-ceramic interface [6], but 70.26%Ag–28.06%Cu–1.68%Ti braze enabled to join h-BN and tungsten carbide.

The reason why the wide distribution of shear strength occurred can be explained by dispersion of ceramics strength. The variation of shear strength followed Weibull distribution as shown in Fig. 14. In both cases, the plot can be approximated by line formula and this indicates that the reason of fracture was originated from single mode. Besides, the fracture was formed in h-BN body near the interface. This result shows that h-BN is a brittle material and that the distribution of shear strength may be wide. In addition, this h-BN used in this study was produced by hot pressing method using high purity plate crystal, so most of grain was oriented to the same direction of shear stress test and its relative density was not so high about 82.5%. This feature resulted in low bulk

strength. Judging from the difference between the two extreme values and low bulk strength, it seemed that the distribution of shear strength of 1.25%Ti to 1.68%Ti was within the margin of variation.

## 5. Concluding remarks

Dissimilar laser brazing of boron nitride and tungsten carbide was done. Observation and structural analysis of its interface and shear strength test revealed as follows:

(1) The contact angles between h-BN and Ag–Cu–Ti braze and between WC–Co and Ag–Cu–Ti braze were acute angle for both brazes containing 1.68%Ti and 1.25%Ti. Wettability of these brazes to h-BN was also considered to be good whenever Ti content in braze was even 1.25%.
(2) At the interface of h-BN/Ag–Cu–Ti braze, braze was observed to infiltrate into micro open pores of h-BN in both cases of using 1.68%Ti braze and 1.25%Ti braze.
(3) At the interface of h-BN/Ag–Cu–Ti braze, concentration of Ti near the interface of which width was about 2 μm was observed in both brazes containing 1.68%Ti and 1.25%Ti. Distribution of N was also observed at same area. It was presumed that the reacted phase existed near the interface between h-BN and braze.
(4) In both brazes containing 1.68%Ti and 1.25%Ti, no large voids or cracks in the braze area were existed from non-destructive observation of the interface using scanning acoustic microscopy.
(5) Fracture occurred at h-BN side of the specimen near the interface in each specimen after shear strength test. It suggests that the shear strength indicates the bulk strength of h-BN and this brazing joint has the strength enough to connect h-BN and WC–Co.

## Acknowledgements

This work was supported by Joint Research system at the Joining and Welding Research Institute, Osaka University, and Grant-in-Aid for Cooperative Research Project of Nationwide Joint-Use Research Institutes on Development Base of Joining Technology for New Metallic Glasses and Inorganic Materials from The Ministry of Education, Culture, Sports, Science and Technology, Japan. The authors would like to thank A. Takezaki (Shin-Ei Seisakusyo Co., Ltd.) for assistance and providing apparatus, brazes and tungsten carbide materials.

## References

[1] Biddulph RH. Boride and carbide ceramics – the systems. In: Proceedings of the 1st European symposium on engineering ceramics; 1985. p. 45–61.
[2] Chattopadhyay AK, Hintermann HE. On brazing of cubic boron nitride abrasive crystals to steel substrate with alloys containing Cr or Ti. J Mater Sci 1993;28(21):5887–93.
[3] Felba J, Friedel KP, Krull P, Pobol IL, Wohlfahrt H. Electron beam activated brazing of cubic boron nitride to tungsten carbide cutting tools. Vacuum 2001;62:171–80.
[4] Sechi Y, Takezaki A, Tsumura T, Nakata K. Dissimilar laser brazing of boron nitride and tungsten carbide. Smart Process Technol 2008;2:27–30.
[5] Nakao Y, Nishimoto K, Saida K. Bonding of $Si_3N_4$ to metals with active filler metals. Trans of J.W.S. 1989;20(1):66–76.
[6] Nicholas MG, Mortimer DA, Jones LM, Crispin RM. Some observations on the wetting and bonding of nitride ceramics. J Mater Sci 1990;25(6):2679–89.
[7] Nakao Y, Nishimoto K, Saida K. Reaction layer formation in nitride ceramics to metal joints bonded with active filler metals. ISIJ Int 1990;30(12):1142–50.
[8] Murakawa M, Takeuchi S. Forming of a grinding wheel using a dresser with brazed diamond film. Mater Sci Eng A 1991;140(01/02):759–63.
[9] Peteves SD. Joining nitride ceramics. Ceram Int 1996;22(6):527–33.
[10] Fernandes AJS, Fonseca MJ, Costa FM, Silva RF, Nazare MH. Ultramicrohardness cross-profiling of CVD diamond/steel brazed junctions. Diamond Relat Mater 1999;8(02/05):855–8.
[11] Huang SF, Tsai HL, Lin ST. Effects of brazing route and brazing alloy on the interfacial structure between diamond and bonding matrix. Mater Chem Phys 2004;84(02/03):251–8.
[12] Rohde M, Suedmeyer I, Urbanek A, Torge M. Joining of alumina and steel by a laser supported brazing process. Ceram Int 2009;35(1):333–7.
[13] Wlosinski W. Interfaces in dissimilar materials joints. Fueg Keram Gla Met 1985:22–36.
[14] Jenney CL, O'Brien A. Welding handbook, vol. 1. American Welding Society; 2001.
[15] Witherell CE, Ramos TJ. Laser brazing. The feasibility of brazing thin sections with minimal distortion and heat input is demonstrated, and rapid solidification rates produce nearly twofold hardness increases for some filler metals. Weld J 1980;59(10):267S–77S.
[16] Hanebuth H, Hoffmann P, Geiger M. Laser beam brazing using the twin spot technology. Proc SPIE Int Soc Opt Eng 1994;2207:146–53.
[17] Whitehead DG, Foster RJ. Soldering with light. Assembly Autom 1995;15(2):17–9.
[18] Dave VR, Carpenter RW, Milewski JO, Christensen DT. Precision laser brazing utilizing non-imaging optical concentration. Weld J 2001;80(6):142.S–7.S.
[19] Markovits T, Takacs J, Lovas A, Belt J. Laser brazing of aluminium. J Mater Process Technol 2003;143/144:651–5.
[20] Vollertsen F, Grupp M. Laser beam joining of dissimilar thin sheet materials. Steel Res Int 2005;76(02/03):240–4.
[21] Saida K, Song W, Nishimoto K. Diode laser brazing of aluminum alloy to steels with aluminum filler metals. Sci Technol Weld Join 2005;10(2):227–35.
[22] Mathieu A, Cicala E, Matteie S, Gewvey D, Pontevicci S, Viala JC. Laser brazing of a steel/aluminium assembly with hot filler wire (88% Al, 12% Si). Mater Sci Eng A 2006;435/436:19–28.
[23] Li MG, Sun DQ, Qiu XM, Sun DX, Yin SQ. Effects of laser brazing parameters on microstructure and properties of TiNi shape memory alloy and stainless steel joint. Mater Sci Eng A 2006;424(1/2):17–22.
[24] Mathieu A, Matteie S, Grevey D, Deschamps A, Martin B. Temperature control in laser brazing of a steel/aluminium assembly using thermographic measurements. NDT E Int 2006;39(4):272–6.
[25] Saida K, Song W, Nishimoto K. Laser brazing of alloy 600 with precious filler metals. Sci Technol Weld Join 2006;11(5):694–700.
[26] Saida K, Song W, Nishimoto K. Theoretical approaches to erosion and wetting phenomena during laser brazing process. Design Interfacial Struct Adv Mater Joints Solid State Phenom (Part B) 2007;127:301–6.
[27] Takemoto T, Kawahito Y, Nishikawa H, Katayama S, Kimura S. Fluxless joining of aluminum alloy to steel by laser irradiation method. J Light Metal Weld Constr 2008;46(7):300–8.
[28] Saida K, Song W, Nishimoto K. Computer simulation of wetting and flowing behaviors of filler metal during laser brazing process. Mater Sci Forum 2008;580/582:271–4.
[29] Weibull W. A statistical distribution function of wide applicability. J Appl Mech 1951;18(3):293–7.
[30] Stanley P, Fessler H, Sivill AD. An engineer's approach to the prediction of failure probability in brittle components. Proc Brit Ceram Soc 1973;22(3):453–87.
[31] Lengauer W, Ettmayer P. The crystal structure of a new phase in the titanium-nitrogen system. J Less-Common Met 1986;120:153–9.
[32] Benko E. Wettability studies of cubic boron nitride by silver–titanium. Ceram Int 1995;21(5):303–7.
[33] Benko E, Bielanska E, Perevertelio VM, Loginova OB. Formation peculiarites of the interfacial structure during cBN wetting with Ag–Ti, Ag–Zr and Ag–Hf alloys. Diamond Relat Mater 1997;6(8):931–4.
[34] Thorsen KA. Applied thermodynamics. Adv Powder Metall Partic Mat 1994;3:183–97.
[35] Elliott JF, Gleiser M. Thermochemistry for steelmaking, vol. 1. Massachusetts: Addison-Wesley; 1960.